Accepted manuscript. Published in Géotechnique (2017). Version of record: https://doi.org/10.1680/jgeot.16.P.181. This is the authors' final version after peer review. Please cite the published article.

A rate-dependent breakage model based on the kinetics of crack growth at the grain scale

Yida Zhang[1] and Giuseppe Buscarnera[2]

ABSTRACT

Experimental evidence indicates that granular soils under high confining stress accumulate deformation over time, with processes such as creep, relaxation and strain-rate sensitivity being controlled by the growth of internal flaws and the delayed fracture of individual particles. In this paper, a connection between the theory of subcritical crack propagation and the continuum modelling of crushable soils is established by exploiting an analogy between the processes that promote energy release upon the fracture of single particles and those that are responsible for delayed comminution in soil samples. Models describing the kinetics of crack propagation have been reinterpreted from a thermodynamic standpoint, showing that the energy loss during crack growth includes higher-order terms which augment the dissipation by surface area creation. Such result has inspired the introduction of similar higher-order terms in the dissipation function of a continuum breakage model, thus hypothesizing that the rate-dependence of collective crushing can be seen as the macroscopic outcome of the growth of cracks in individual grains. This choice leads to a rate-dependent continuum model characterized by a breakage growth rate controlled by the same coefficient that governs the kinetics of crack growth in the grain-forming minerals (the so-called stress corrosion index). It is shown that the model exhibits good agreement with the creep and relaxation response measured for a range of soils tested under oedometric and triaxial conditions. These results corroborate the hypotheses about the link between subcritical crack growth and the energetics of delayed comminution and set a vision to model delayed fracture processes occurring in fluid-infiltrated reactive environments.

INTRODUCTION

The rate-dependent behaviour of granular materials plays an important role in numerous phenomena, such as delayed settlements in rockfill dams (Oldecop and Alonso, 2007), creep in pile foundations (Leung et al., 1997) and temporal evolution of the penetration resistance of sandy deposits (Michalowski and Nadukuru, 2012). Recent studies have also pointed out that the viscoplastic deformation of granular geomaterials may be involved in the long-term subsidence due to fluid withdrawal from weakly consolidated reservoirs (Chan,

[1] University of Colorado Boulder, Department of Civil, Environmental and Architectural Engineering, Boulder, CO, USA. Formerly Ph.D. Candidate, Northwestern University, Department of Civil and Environmental Engineering, Evanston, IL, USA.

[2] Northwestern University, Department of Civil and Environmental Engineering, Evanston, IL, USA

2004; Fisher et al., 1999). While numerous microscopic processes at low and/or high pressures influence the rate-dependent behaviour of granular soils (Tatsuoka et al., 2002; 2008), in the examples mentioned above the system response is controlled by the fragility of the grains, thus having the delayed breakage of individual particles as a key component in the rearrangement of the skeleton over time, as well as in the rates of creep and stress relaxation (Karimpour and Lade, 2010). The understanding of such phenomena requires a comprehensive inspection of rate-effects at both macroscopic and particle scales. Oedometric and triaxial tests on sand specimens illustrate indeed that their stress-strain response is rate-dependent and cannot be modelled by a unique relation between stresses, strains and strain-rates (so-called *nonisotach* behaviour; Tatsuoka et al., 2002; Augustesen et al., 2004). Such complex rate-dependence has led to detailed measurements of evolving particle size distribution during creep and relaxation tests (Leung et al., 1997; Lade et al., 2010) and it has inspired micromechanical interpretations of environment-dependent creep based on the theory of crack growth kinetics (Oldecop and Alonso, 2001; 2007), i.e. delayed processes observed in brittle solids such as glasses, ceramics and rocks, for which the terms *static fatigue* (Scholz, 1972) or *subcritical fracture* (Atkinson, 1982) are often interchangeably adopted. By using these theories, it is possible to calculate the failure time of grains subjected to diametrical compression as a function of the fracture properties of the constituting mineral (Oldecop and Alonso, 2007). However, the application of subcritical crack growth theories to the continuum modelling of time effects in soils has been hindered by the widely different length scales involved in the process, as well as by a substantial detachment between the continuum models for granular soils and the physics of fracture. For example, macroscopic models for sands incorporating time effects have primarily relied on critical state elasto-viscoplasticity (Yin and Graham, 1999) or rheological laws based on spring-dashpot systems (Tatsuoka et al., 2002). These models often display good agreement with data, but at the cost of numerous parameters of unclear physical meaning.

An alternative avenue to model the deformation response of granular soils relies on the direct incorporation of micromechanical arguments, and it has been recently explored with significant success in the context of

grain crushing. A notable example is the *Breakage Mechanics* theory proposed by Einav (2007a), i.e. a continuum thermodynamic approach sharing numerous similarities with the energetics of fracture initiation (Griffith, 1921). Given its ability to account for grain-scale geometric attributes (e.g., average grain size, degree of polydispersity, specific surface area), this line of modelling has been exploited to study physico-chemical interactions between grain skeleton and fluids (Buscarnera and Einav, 2012; Buscarnera and Das, 2015; Buscarnera, 2012), and has been enhanced by Zhang et al. (2016) by accounting for the connection between the fracture of single particles and the work input required to trigger crushing across a specimen.

All such theories rely on a rate-independent description of grain crushing in soils, thus implicitly assuming instantaneous fragmentation and lack of static fatigue. As a result, the study of the implications of delayed fracture in this class of models is largely unexplored, and requires an overarching interpretation of the interplay between intra-grain crack growth and delayed comminution. In this paper, a rate-dependent breakage model is formulated by exploiting an analogy between the dissipation rate functions of two distinct irreversible processes: (i) the propagation of particle flaws and (ii) the development of breakage in a compressed assembly. For this purpose, existing models available to simulate subcritical crack growth are reviewed, discussing their ability to capture evidences of fracture propagation in solids under tension. Then, a specific fracture kinetics law is inspected from a thermodynamic standpoint, with the goal to derive a dissipation function valid for systems prone to tensile fracture (e.g., particles under diametrical compression). By comparing such dissipation function with the loss of energy by surface area creation in Griffith-like cracks, a strategy to augment the constitutive laws of a rate-independent continuum breakage model is proposed. Specifically, a non-homogeneous form of breakage dissipation is suggested, in which the degree of non-linearity is hypothesized to be a function of the constants that control the crack growth rate at the scale of particle flaws. Such hypothesis leads to a one-dimensional rate-dependent model with a mathematical structure inspired by both subcritical crack growth theories and rate-independent Breakage

laws. Finally, the model is extended to triaxial states of stress and is tested against experimental data reported for a number of granular soils subjected to high compressive stresses.

SUBCRITICAL CRACK PROPAGATION

Subcritical crack growth refers to the extension of cracks at values of energy release rate that are lower than the critical threshold for catastrophic crack propagation (Atkinson and Meredith, 1987). Such phenomenon has been observed in glasses, ceramics, quartz and various types of natural rocks, and it is highly sensitive to environmental factors such as relative humidity and temperature (Wiederhorn, 1967; Atkinson, 1982). Figure 1a shows a typical plot of crack propagation velocity, $\dot{l}$, as a function of the stress intensity factor for mode I, K_I, in presence of various degrees of water vapour concentration. From such figure, three crack growth regimes can be identified, all located at values of K_I greater than K_{I0} (often referred to as *stress corrosion limit*). Region I, is the regime where the crack velocity increases exponentially, and it is assumed to be controlled by the reaction rate between environmental species and strained bonds in proximity of the crack tip (thus making $\dot{l}$ dependent on both K_I and chemical conditions). At higher values of K_I (region II), where $\dot{l}$ displays a much weaker dependence on K_I, the diffusion of the reactive species towards the crack tip is often hypothesized to govern the crack propagation velocity. Finally, in region III K_I approaches the critical value K_{IC} in vacuum, at which the crack propagates catastrophically without displaying any noticeable dependence on the environmental agents. Based on such observation, many kinetic models have been proposed (see Atkinson and Meredith (1987) for a review). Among them, the Charles equation (Charles, 1958) has been widely applied to interpret subcritical crack growth data. A possible form to express such a simple kinetics law is given as follows (Oldecop and Alosno, 2007):

$$\dot{l} = \dot{l}_0 \left(\frac{K_I}{K_{Iref}} \right)^n \tag{1}$$

where n is the stress corrosion index (i.e., the constant controlling the rate of crack advancement); $\dot{l}_0$ is a reference crack propagation velocity; and K_{Iref} is a stress intensity factor used for normalization purposes (which depending on convenience may be either the fracture toughness under vacuum, K_{IC}, or the minimum stress intensity factor for fracture growth under the prevailing environmental conditions, K_{I0}). The Charles equation satisfactorily models the crack growth behaviour observed in region I for most minerals and rocks. For example, Figure 1b collects $K_I - \dot{l}$ diagrams for synthetic quartz and quartz-rich rocks subjected to different environmental conditions, and it shows that the values of n may vary between 15 and 60.

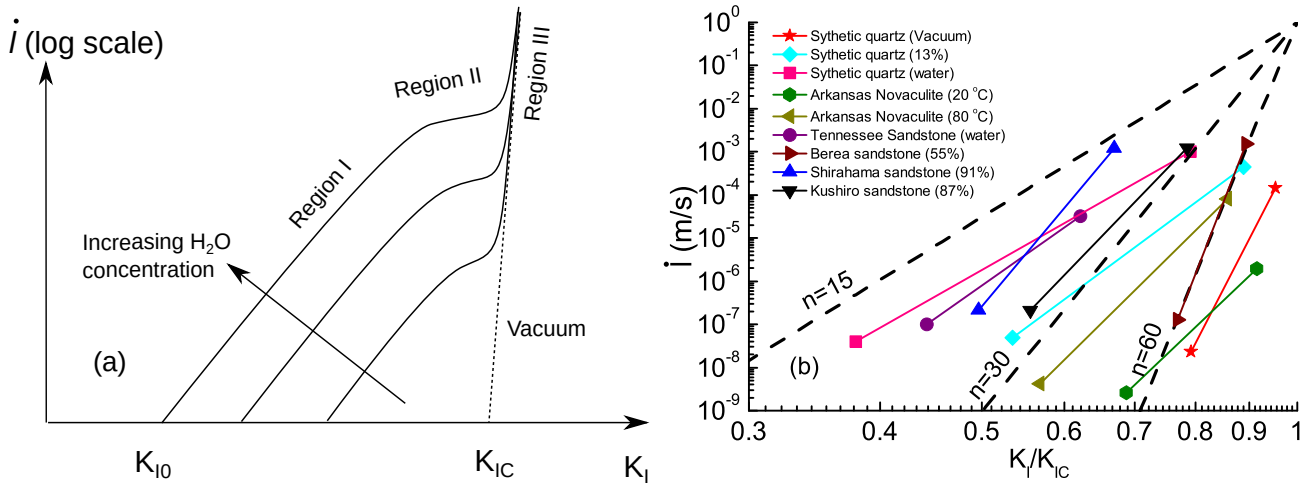

Figure 1: a) Typical stress corrosion curves represented in the $K_I - \dot{l}$ plane (after Atkinson and Meredith, 1987); b) $K_I - \dot{l}$ diagrams for quartz-rich rocks exposed to various environmental conditions. The dash lines represent the Charles equation used with $K_{Iref}=K_{IC}$ and $\dot{l}_0 = 1$ m/s (data from Atkinson (1980), Atkinson (1984) and Nara et al. (2012)).

A limitation of the Charles equation is that it implies crack extension in presence of any magnitude of stress concentration. In other words, it does not have a stress corrosion limit below which the growth of a crack ceases. Such limit, however, is necessary to explain the rate of crack growth in glasses at low values of stress intensity factor (Figure 2, Wiederhorn and Bolz, 1970), and its existence has also been hypothesized for rocks (Atkinson and Meredith, 1987). An alternative model that includes a stress corrosion limit was proposed by Maugis (1985), and it can be expressed through the following kinetic relation:

$$\dot{l} = \frac{1}{\alpha^{1/n'}} \left\langle \frac{K_I^{\,2}}{K_{I0}^{\,2}} - 1 \right\rangle^{1/n'} \qquad (2)$$

where α and n' are two model parameters and the Macauley brackets are used to limit the discussion to crack growth processes (i.e., $\dot{l} > 0$). It is readily apparent that such model imposes a threshold value of K_I below which the growth of a crack is not possible (i.e., $K_I < K_{I0}$). By specifying the following relations between the parameters of equations (1) and (2):

$$n' = \frac{2}{n}; \alpha = \frac{1}{\dot{l}_0^{2/n}} \tag{3}$$

it is possible to show that the Charles and Maugis equations have the same asymptotic behaviour at large values of K_I:

$$\lim_{K_I \to \infty} \left[\dot{l}_0 \left(\frac{K_I}{K_{I0}} \right)^n \right] \Bigg/ \left[\frac{1}{\alpha^{1/n'}} \left\langle \frac{K_I^{\,2}}{K_{I0}^2} - 1 \right\rangle^{1/n'} \right] = 1 \tag{4}$$

where Equation (1) has been used with $K_{Iref}=K_{I0}$. Thus, the Maugis equation can be expressed in terms of the widely used parameters of the Charles law, as follows:

$$\dot{l} = \dot{l}_0 \left\langle \frac{K_I^{\,2}}{K_{I0}^2} - 1 \right\rangle^{n/2} = \dot{l}_0 \left\langle \frac{G_I}{2\gamma} - 1 \right\rangle^{n/2} \tag{5}$$

where G_I is the energy release rate (which in linear elastic solids is proportional to the square of K_I) and γ is the solid surface energy related with the initiation of crack growth under the considered environmental conditions. Figure 2a shows a plot of the Charles and Maugis equations on a double-logarithmic scale, from which the convergence of the two models at large values of K_I is readily apparent. While both laws depict a subcritical crack growth with the same corrosion index (n=10), the Maugis equation also imposes a stress corrosion limit (K_{I0}=0.1 MPa·m$^{0.5}$). Figure 2b illustrates the importance of such limit with reference to data reported by Wiederhorn and Bolz (1970). It can be noted that the non-linearity of the crack growth process in proximity of the stress corrosion limit is accurately captured by Equation (5), which therefore offers both conceptual and practical advantages. Specifically, the presence of an initiation threshold offers the

possibility to reinterpret the Maugis model in light of thermodynamic arguments (Rice, 1978) and it enables the inspection of the dissipative processes associated with delayed fracture.

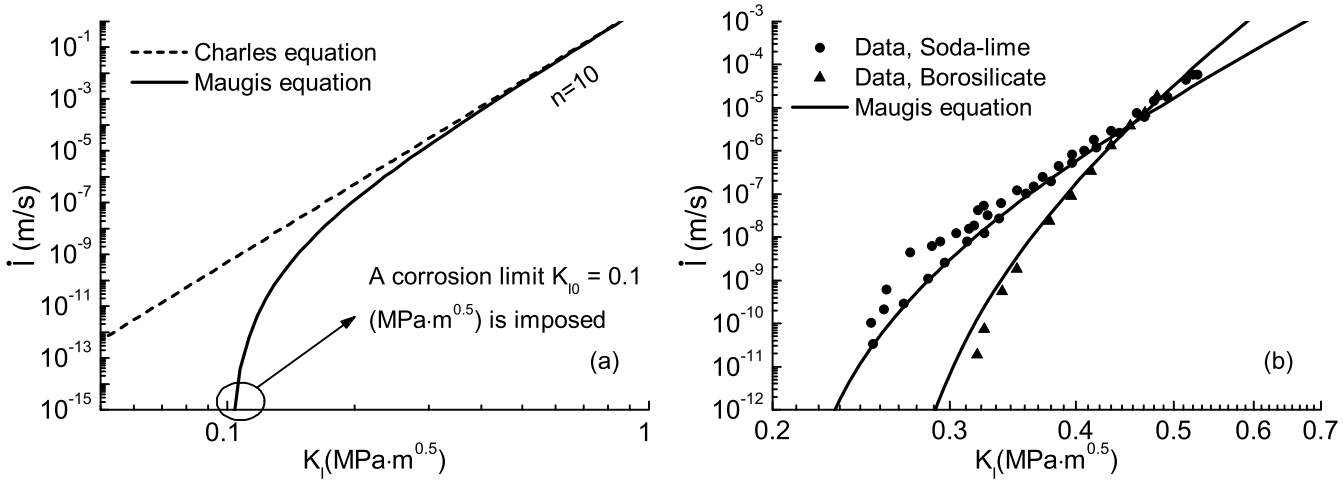

Figure 2: a) Typical plot of Charles and Maugis crack propagation equation (K_{I0}= 0.1 MPa·m$^{0.5}$, n = 10 and $\dot{l}_0 = 5\times10^{-10}$ m/s); b) Interpretation data for soda-lime and borosilicate glass (Wiederhorn and Bolz, 1970) through the Maugis equation (K_{I0}= 0.2 MPa·m$^{0.5}$, n = 12 and $\dot{l}_0 = 8\times10^{-10}$ m/s for soda-lime glass; K_{I0}= 0.25 MPa·m$^{0.5}$, n = 16 and $\dot{l}_0 = 5\times10^{-9}$ m/s for borosilicate glass).

DISSIPATION IN SUBCRITICAL CRACK GROWTH

Dissipative processes such as crack propagation can be interpreted in light of the thermodynamics with internal variables (TIV). Such framework is a versatile tool to describe irreversible processes in the vicinity of equilibrium and provides a framework to establish kinetic equations obeying the second law of thermodynamics. Depending on the chosen extremal principles, the evolution equations can be defined by postulating either a non-negative dissipation rate function Φ, a force potential z or a flow potential w (Houlsby, 2014). These potentials can be converted to each other when certain mathematical requirements are fulfilled (Hackl and Fischer, 2008; Houlsby and Puzrin, 2007). As a result, it is often sufficient to specify only one of them to formulate a complete inelastic constitutive model. A remarkable example is the case of Φ homogeneous function of degree 1, for which the corresponding force potential z coincides with Φ, the flow potential collapses into a yield function (w=0), and the evolution equations become rate-independent (Houlsby, 2014). The procedure to derive evolution laws through such formalism, as well as the mathematical relations between Φ, z and w, are briefly summarized in Appendix 1.

Here, subcritical crack growth is treated as a particular rate-dependent dissipative process, thus recasting it into the framework of TIV. Appropriate expressions of Φ, z and w will be inferred from evidences available about the kinetics of fracture in brittle solids. For this purpose, let us consider a disk-shaped particle with a central flaw subjected to diametrical compression (Figure 3). To consider a 2D analysis, the disk is assumed to have unitary thickness in the out of plane direction (the extension to a 3D case would imply only minor changes, such as making reference to a propagating crack front of arbitrary shape; see for example Rice (1978)). The state of the selected system can be characterized by an external variable Δ (representing the reversible displacement of the loading plate) and an internal variable l (representing the length of the crack, here assumed to be monotonically increasing). Isothermal conditions are assumed, thus including the possibility of heat exchanges with the environment (e.g., the heat flow **Q** in Figure 3). The first law of thermodynamics therefore states:

$$W = \dot{\Psi} + \Phi \tag{6}$$

where $W = P\dot{\Delta}$ is the rate of work input to the system, P the compressive load, $\Psi = \Psi(\Delta, l)$ the Helmholtz free energy (i.e., the strain energy stored in the particle) and Φ the dissipation rate function.

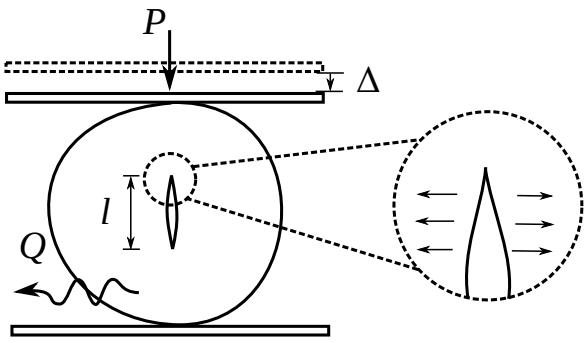

Figure 3: Schematic diagram of fracturing process in disk-shaped particle with centre crack. A tensile stress field is assumed to prevail in the vicinity of the crack tip, thus considering a scenario of mode I crack propagation.

Assuming that the energy is dissipated only as a consequence of fracture initiation/propagation, Φ can be decomposed into two parts, as follows:

$$\Phi(\dot{l}) = 2\gamma\dot{l} + \phi_C(\dot{l}) \geq 0 \tag{7}$$

where the first term represents the energy lost by new surface area creation, while ϕ_C reflects an additional energy dissipation term associated with the propagation of a crack over time (here assumed to depend only on the crack growth rate). Indeed, the loss of energy by surface area creation is always accompanied by additional dissipation mechanisms, which may include wave emission (Boudet et al., 1996), heat generation (Döll, 1984), solid-environment reactions at crack surfaces (Michalske and Freiman, 1982) or viscoelastic/plastic deformations in the vicinity of the crack tip (Weidmann and Holloway, 1974). To implicitly incorporate such further sources of dissipation, here the non-negativity of $\phi_C \geq 0$ is postulated, which implies a stronger constraint, based on which this term will always augment the energy loss by surface area creation in Equation (7).

Substituting (7) into (6), one obtains the following condition for any admissible processes:

$$\left(P - \frac{\partial\Psi(\Delta,l)}{\partial\Delta}\right)\dot{\Delta} - \left(\frac{\partial\Psi(\Delta,l)}{\partial l} + 2\gamma\right)\dot{l} = \phi_C(\dot{l}) \geq 0 \tag{8}$$

Considering the definition of elastic strain energy $P = \partial\Psi / \partial\Delta$, the following quasi-static crack propagation criterion can be derived:

$$\left(G_I - 2\gamma\right)\dot{l} \geq 0 \tag{9}$$

where $G_I = -\partial\Psi / \partial l$ is the energy release rate associated with the extension of the crack. The condition above is identical to the crack growth criterion derived by Rice (1978) for fractured solids under tensile loading. Equation (9) recovers the Griffith criterion for the case in which only crack growth is allowed (i.e., $\dot{l} \geq 0$), having that:

$$\begin{cases} \dot{l} = 0 & \text{for} \quad 0 \leq G_I < 2\gamma \\ \dot{l} \geq 0 & \text{for} \quad G_I \geq 2\gamma \end{cases} \tag{10}$$

If it is assumed that the strain energy is dissipated solely by surface area creation (i.e., ϕ_C=0), (7) becomes homogeneous of degree 1, thus corresponding to a rate-independent fracture process for which a fracture initiation threshold, y_C, can be derived from a degenerate Legendre transformation (i.e., w=0 in (47)):

$$y_C = \frac{G_I}{2\gamma} - 1 = 0 \tag{11}$$

Such criterion bounds the reversible regime in Equation (9) and represents a yield surface for the fracture process expressed in energy terms.

Now let us consider the case in which the creation of surface area is accompanied by additional sources of dissipation (i.e., $\phi_C > 0$). Here a particular case is considered where ϕ_C is expressed as a power law function of $\dot{l}$, as follows:

$$\phi_C(\dot{l}) = 2\gamma \dot{l} \left(\frac{\dot{l}}{\dot{l}_0} \right)^{2/n} \tag{12}$$

through which $\Phi(\dot{l})$ in (7) becomes:

$$\Phi(\dot{l}) = 2\gamma \dot{l} \left(1 + \left(\frac{\dot{l}}{\dot{l}_0} \right)^{2/n} \right) \geq 0 \tag{13}$$

and the force potential z can be found through equation (50):

$$z = 2\gamma \dot{l} + \frac{2\gamma \dot{l}}{2/n+1} \left(\frac{\dot{l}}{\dot{l}_0} \right)^{2/n} \tag{14}$$

Consequently, the thermodynamic force G_I conjugated to $\dot{l}$ can be derived through (46):

$$G_I = \frac{\partial z}{\partial \dot{l}} = 2\gamma \left[1 + \left(\frac{\dot{l}}{\dot{l}_0} \right)^{2/n} \right] \geq 0 \tag{15}$$

Inversion of (15) leads to a fracture kinetics relation. For $0 \le G_I < 2\gamma$, the constraint (9) is satisfied only if $\dot{l} = 0$, thus implying lack of crack growth. By contrast, for $G_I \ge 2\gamma$ equation (15) has a real non-negative solution for $\dot{l}$. Therefore, the inverse of equation (15) can be concisely expressed as:

$$\dot{l} = \dot{l}_0 \left\langle \frac{G_I}{2\gamma} - 1 \right\rangle^{n/2} = \dot{l}_0 \xi_C^{\,n/2} \tag{16}$$

This result, here derived from a purely thermodynamic standpoint, is identical to the Maugis kinetics law in Equation (5). The dimensionless term:

$$\xi_C = \left\langle \frac{G_I}{2\gamma} - 1 \right\rangle \tag{17}$$

can be interpreted as an energy-based overstress function similar to those used in Perzyna-type viscoplastic models (i.e., $\xi_C = 0$ represents the rate-independent fracture threshold, y_C, and increasing values of ξ_C tend to produce higher crack growth velocities). For such reason, ξ_C will be hereafter referred to as *fracture overstress function*. For completeness, the flow potential w corresponding to (13) and (14) can be derived by using equation (47):

$$w(G_I) = \Phi(\dot{l}) - z\left(\dot{l}\right) = \frac{2\gamma \dot{l}_0 \xi_C^{\,n/2+1}}{n/2+1} \tag{18}$$

It is worth noting that, although the relations above have been derived from a postulate about the dissipation function Φ, an equivalent strategy would have been to propose directly expressions of z and/or w compatible with the kinetics law in equation (5) (and, hence, having analytical forms similar to those in (14) or (18)).

The above derivation reveals a connection between Rice's interpretation of Griffith's fracture criterion and the Maugis crack growth law. The latter is indeed a consequence of a higher order homogenous term added to the dissipation of a rate-dependent fracture process, which augments the loss of energy via creation of new surface area by accounting for further dissipative processes. Such result inspires a strategy to convert

a rate-independent initiation criterion (e.g., a yield surface) into a rate-dependent evolution law controlled by delayed fracturing (i.e., a kinetic relation), and it will be applied hereafter to the continuum modelling of particle breakage.

DISSIPATION IN ISOTROPIC COMMINUTION

The growth of subcritically stressed cracks in a particle under sustained stress leads to a finite survival time, and recent works by Oldecop and Alonso (2001; 2007) have shown how such time effects contribute to the macroscopic phenomenology of granular creep. Indeed, the time required to split a particle subjected to an external load P can be estimated by integrating the corresponding crack growth velocity with respect to time (Figure 4a). Depending on the magnitude of K_I generated by the load P, the particle can crush catastrophically (i.e. $K_I \geq K_{IC}$), fracture after a finite time (i.e. $K_{I0} < K_I < K_{IC}$) or remain intact indefinitely (i.e. $K_I \leq K_{I0}$). Now let us consider a sand specimen subjected to sustained confining stress (i.e., a creep test). Critically loaded particles arranged along the major force chains will be rapidly crushed. These events are reflected macroscopically as instantaneous inelastic strains developed upon the application of a load increment. The rest of the particles are either stressed with intermediate values of K_I or slightly stressed with $K_I \leq K_{I0}$. As time progresses, the particles under sufficiently high stresses will be consecutively crushed, thus initiating grain rearrangement and force redistribution. Eventually, a stable configuration is achieved where most of the flaws within the particles are stressed below the corrosion limit and only limited strain accumulation is displayed over time (Figure 4b).

According to these considerations, the energy dissipation by macroscopic crushing should not only contain the dissipation associated with the creation of new surface area and the associated energy redistribution, but it should also include additional sources of energy loss that reflect the net dissipation due to delayed inelastic interactions at the crack tips. For this purpose, let us describe the macro-scale energetics of comminution in granular soils through the Breakage Mechanics theory (Einav, 2007a, b), i.e. a framework expressing the dissipation due to distributed crushing in terms of the evolution of the grain size distribution (see Appendix

2 for more details). In case of negligible macroscopic plastic strains (a simplifying hypothesis not affecting the following discussion and which will be later removed), the state of a soil subjected to an isotropic state of stress can be fully described by the external state variable ε_v (the volumetric strain, here coinciding with the elastic volumetric strain) and the breakage state variable B (which spans from B=0 for an assembly of unbroken particles to B=1 for a fully crushed state). In analogy with Equation (7), the dissipation rate function is here proposed to have the following structure:

$$\Phi(B,\dot{B}) = \frac{E_c \dot{B}}{(1-B)^2} + \phi_B(\dot{B}) \geq 0 \tag{19}$$

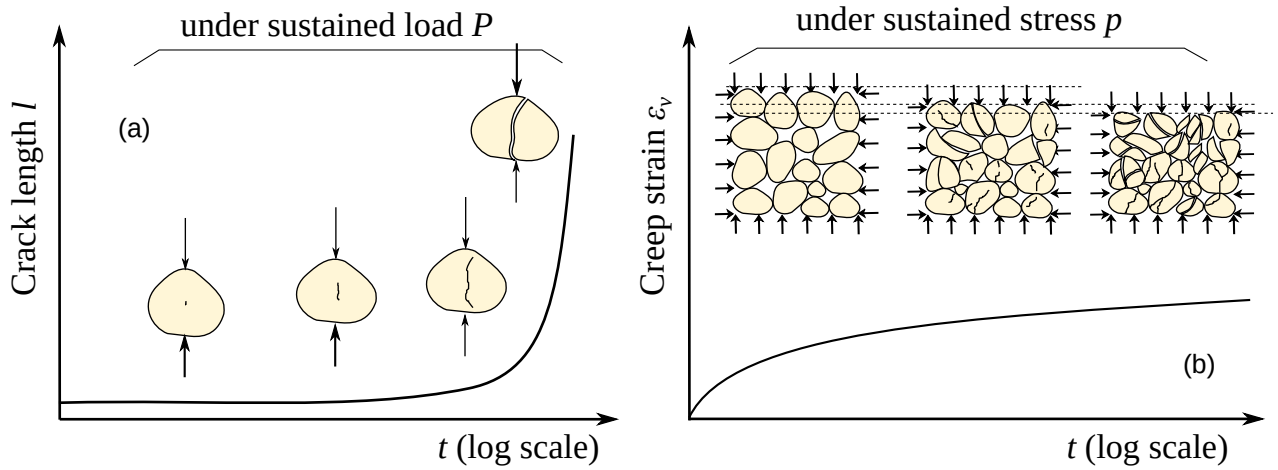

Figure 4: Schematic diagrams of a) fracture growth in a subcritically loaded particle and b) creep in a granular assembly

where E_c is a material constant referred to as *critical breakage energy*. The first term on the right hand side of (19) is the breakage dissipation accounting for the creation of new surface area, as well as the associated loss of energy due to force redistribution (Einav, 2007a). By contrast, the second term $\phi_B \geq 0$ collects additional dissipative terms due to stress corrosion at crack tips and delayed breakage. Considering the work input of the system $W = p\dot{\varepsilon}_v$ and a total Helmholtz free energy expressed in the form $\Psi = \Psi(B, \varepsilon_v)$, the following thermodynamic relation can be derived:

$$\left(p - \frac{\partial \Psi(\varepsilon_v, B)}{\partial \varepsilon_v}\right)\dot{\varepsilon}_v - \left(E_B - \frac{E_c}{(1-B)^2}\right)\dot{B} = \phi_B(\dot{B}) \geq 0 \tag{20}$$

where $E_B = -\partial\Psi / \partial B$ is the breakage energy representing the energy release rate due to an infinitesimal change of the grain size distribution and p is the mean stress. In the absence of stress corrosion effects (i.e. $\phi_B = 0$), Equation (19) becomes a homogenous function of degree 1 and the isotropic breakage process is rate-independent. The breakage criterion can be derived by reorganizing (20) and taking into account the hyperelastic relation $p = \partial\Psi / \partial\varepsilon_v$ (Einav, 2007a):

$$y_B = \frac{(1-B)^2 E_B}{E_c} - 1 = 0 \tag{21}$$

Delayed effects can be incorporated by assuming non-zero values for the dissipation term ϕ_B. By analogy with the kinetics laws discussed in the previous section, it is expected that ϕ_C and ϕ_B share a similar mathematical structure due to the fact that the latter represents the smeared outcome of distributed fracture events taking place in the subcritical crack growth regime. Particularly, here it is hypothesized that ϕ_C and ϕ_B have the same order of nonlinearity with respect to their thermodynamic velocities $\dot{l}$ and $\dot{B}$, respectively. In other words, ϕ_B is proposed to have the following expression:

$$\phi_B(\dot{B}) = \frac{E_c \dot{B}}{(1-B)^2}\left(\frac{\dot{B}}{\dot{B}_0}\right)^{2/n} \tag{22}$$

where $\dot{B}_0$ is a reference breakage growth rate. The total dissipation rate function now becomes:

$$\Phi(B,\dot{B}) = \frac{E_c \dot{B}}{(1-B)^2}\left(1+\left(\frac{\dot{B}}{\dot{B}_0}\right)^{2/n}\right) \tag{23}$$

in which the rate-independent dissipation is augmented by a multiplicative factor taking a similar form to that used in Equation (13). The force potential corresponding to (23) is:

$$z(B,\dot{B}) = \frac{E_c \dot{B}}{(1-B)^2}\left(1+\frac{1}{2/n+1}\left(\frac{\dot{B}}{\dot{B}_0}\right)^{2/n}\right) \tag{24}$$

from which the expression of E_B is readily derived:

$$E_B = \frac{\partial z}{\partial \dot{B}} = \frac{E_c}{(1-B)^2}\left[1+\left(\frac{\dot{B}}{\dot{B}_0}\right)^{2/n}\right] \tag{25}$$

Values of breakage energy between $0 \le E_B < E_c/(1-B)^2$ correspond to the elastic regime bounded by the criterion (21), and indicate values of breakage growth rate $\dot{B}$ equal to zero. When $E_B \ge E_c/(1-B)^2$, equation (25) provides real non-negative solutions for $\dot{B}$. Thus the breakage evolution law obtained by inverting equation (25) can be concisely expressed as:

$$\dot{B} = \dot{B}_0\left\langle \frac{(1-B)^2 E_B}{E_c} - 1 \right\rangle^{n/2} = \dot{B}_0 \xi_B{}^{n/2} \tag{26}$$

where the dimensionless term

$$\xi_B(B,E_B) = \left\langle \frac{(1-B)^2 E_B}{E_c} - 1 \right\rangle \tag{27}$$

can be regarded as a *breakage overstress function*. An alternative approach to define breakage evolution is to construct a flow potential w by directly making an analogy to that of crack growth (18):

$$w\left(B,E_B\right) = \frac{E_c \dot{B}_0}{\left(1-B\right)^2}\frac{\xi_B{}^{n/2+1}}{n/2+1} \tag{28}$$

It can be easily checked that the derivative of w with respect to E_B generates the same breakage evolution equation in that (28) corresponds to the Legendre transform of z in (24).

Combining Equations (16) and (26), one obtains the following relation:

$$\frac{\log\left(\dot{I}/\dot{I}_0\right)}{\log \xi_C} = \frac{\log\left(\dot{B}/\dot{B}_0\right)}{\log \xi_B} = \frac{n}{2} \tag{29}$$

Equation (29) displays the implications of having used the same order of nonlinearity for ϕ_C and ϕ_B. In particular, according to (29) the corrosion index n not only governs the kinetics of crack propagation within the grains, but it also enters in the continuum description of the rate-dependent crushing of an assembly. This hypothesis results in the same logarithmic growth of the internal variables $\dot{I}$ and $\dot{B}$ when plotted against their respective overstress functions ξ_C and ξ_B (Figure 5). The applicability of such convenient hypothesis will be discussed in the subsequent sections with reference to laboratory evidences.

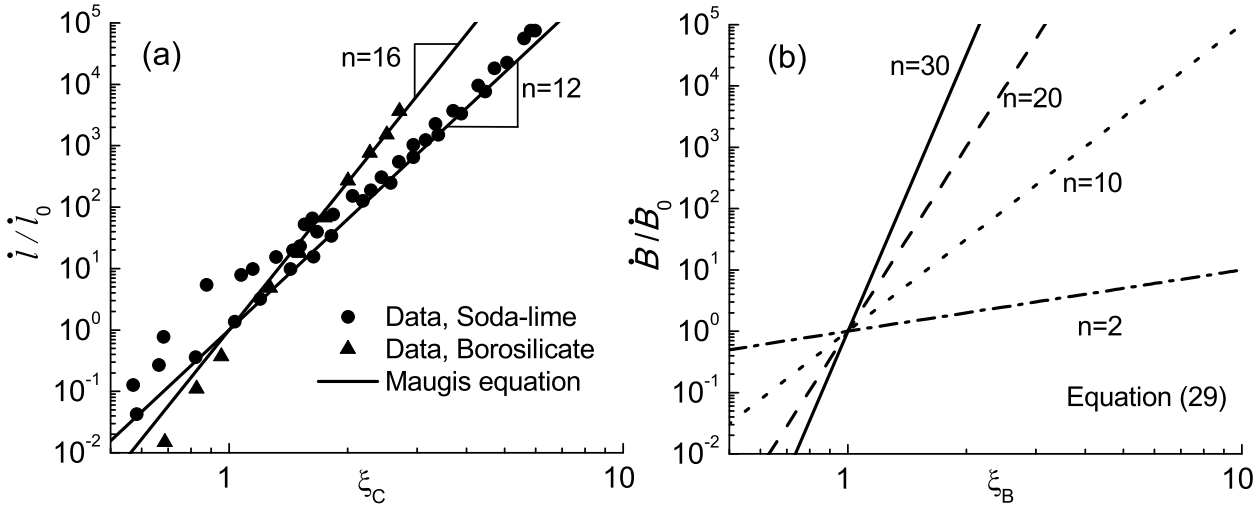

Figure 5: a) Plot of Maugis model and subcritical crack growth data on the $\dot{I}/\dot{I}_0 - \xi_C$ plane; b) visualization of Equation (29) for different values of n.

SIMPLE ISOTROPIC MODEL FOR RATE-DEPENDENT BREAKAGE

Some key properties of the rate-dependent breakage theory derived in the previous section are illustrated here with reference to isotropic stress conditions. For this purpose, let us consider a simple linear elastic model based on the following Helmholtz free energy potential:

$$\Psi(B,\varepsilon_v) = \frac{1}{2}\left(1-\vartheta B\right) K \varepsilon_v^2 \tag{30}$$

where the term $(1-\vartheta B)$ derives from a statistical homogenization procedure (Einav, 2007a) and ϑ is a grading index that can be computed from the initial and ultimate grain size distribution (see Appendix 2). The elastic constitutive relations can be obtained through hyperelastic relations:

$$p = \frac{\partial \Psi}{\partial \varepsilon_v} = \left(1-\vartheta B\right) K \varepsilon_v \tag{31}$$

$$E_B = -\frac{\partial \Psi}{\partial B} = \frac{1}{2} K \vartheta \varepsilon_v^2 = \frac{1}{2} \frac{\vartheta p^2}{K\left(1-\vartheta B\right)^2} \tag{32}$$

The stress rate can be further derived as:

$$\dot{p} = \left(1-\vartheta B\right) K \dot{\varepsilon}_v - K \vartheta \varepsilon_v \dot{B} \tag{33}$$

Considering constant stress condition (i.e. $\dot{p} = 0$), the rate of creep strain can be derived by combining (26), (32) and (33):

$$\dot{\varepsilon}_v = \frac{\dot{B}_0 \vartheta p}{K\left(1-\vartheta B\right)^2} \left\langle \left(\frac{1-B}{1-\vartheta B}\right)^2 \frac{\vartheta p^2}{2KE_c} - 1 \right\rangle^{n/2} \tag{34}$$

Similarly, one can derive the rate of stress relaxation under constant strain conditions (i.e., $\dot{\varepsilon}_v = 0$):

$$\dot{p} = -K \vartheta \varepsilon_v \dot{B}_0 \left\langle \frac{(1-B)^2 K \vartheta \varepsilon_v^2}{2E_c} - 1 \right\rangle^{n/2} \tag{35}$$

Figures 6a and b show a series of constant strain rate simulations, from which it can be observed that the rate-sensitivity can be amplified by reducing either n or $\dot{B}_0$. The two parameters, however, alter the patterns of rate-dependence in very different ways. In particular, $\dot{B}_0$ shifts the stress-strain curves associated with different strain rates of a roughly equal magnitude without affecting significantly their shape. By contrast the parameter n affect both shape and location of these curves. As a result, the characteristics of the predicted

compression behaviour change drastically with an increase or a decrease of the rate of deformation when n=2 is used (thus modelling a strongly viscous behaviour that is rarely observed in experiments on sands), while they maintain similar characteristics at all strain rates if a realistic value of corrosion index (e.g., n=15) is used to reproduce a weakly viscous behaviour.

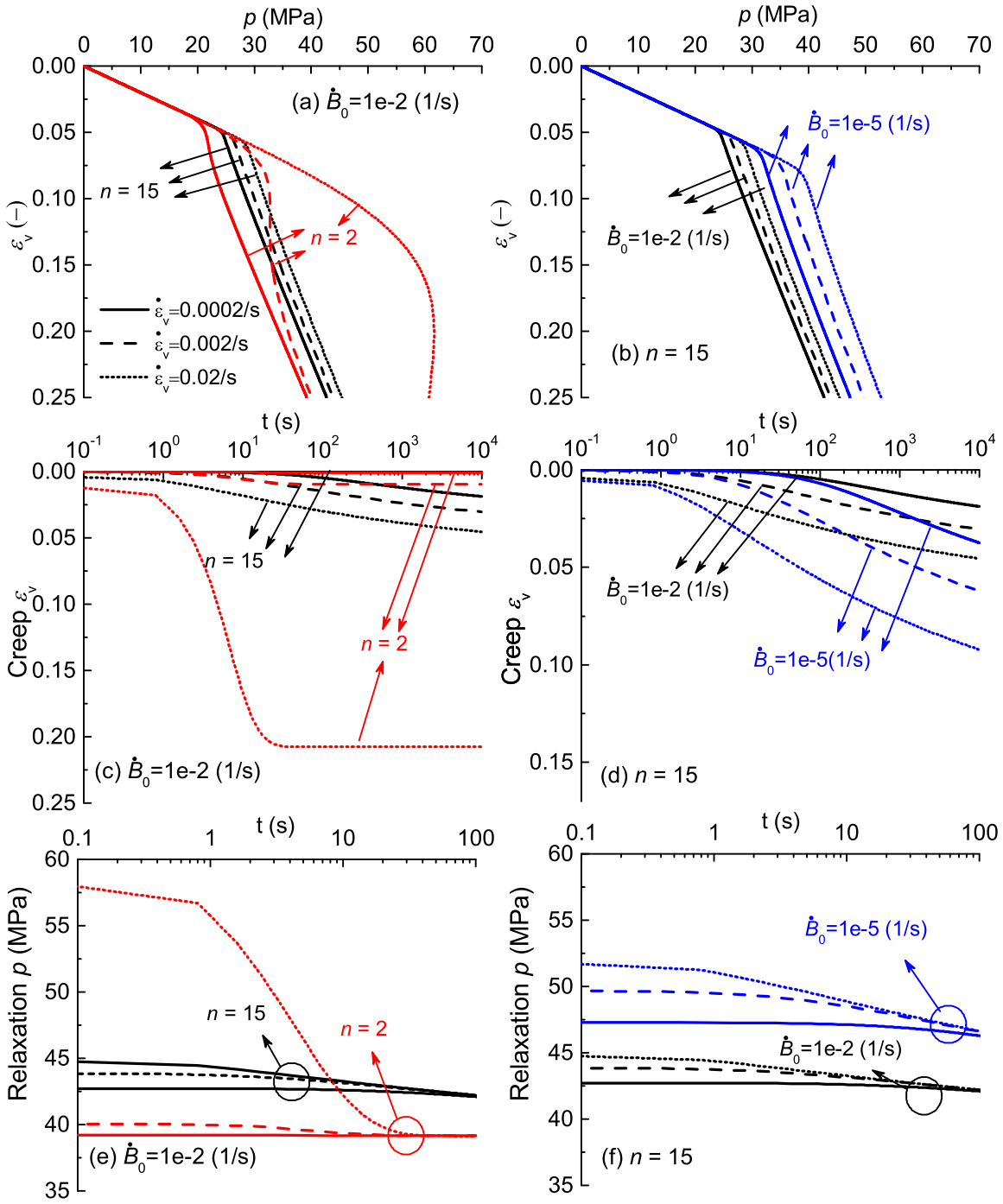

Figure 6: Examples of isotropic breakage simulations exploring the effect of the parameters n and $\dot{B}_0$ under (a,b) constant strain rate tests, (c, d) creep tests and (e, f) relaxation tests (analyses based on ϑ=0.8, E_c=0.25 MPa and K=500MPa,).

Figures 6c and 6d present creep tests conducted at the end of the compression stages, displaying predicted creep histories strongly dependent on the rate of preloading. It is observed again that $\dot{B}_0$ shifts the creep strain curves equally, while *n* changes both their shape and the magnitude of the delayed strains. Figures 6e and 6f finally show the predicted relaxation responses simulated after completion of the compression stages. In addition to confirming the previous observations, the model predicts the convergence of the stresses after certain time of relaxation. However, while for *n*=2 such convergence is achieved only when the delayed effects have already vanished, in case of *n*=15 the curves converge when a logarithmic trend of relaxation is still present, thus displaying a similar pattern of stress decay for a longer time span. The latter pattern of behaviour has been indeed observed in relaxation tests conducted under triaxial conditions (Lade and Karimpour, 2014), and it corroborates the hypothesis that the values of corrosion index usually observed for brittle minerals represent an adequate choice to constrain the degree of non-linearity of the viscous response of crushable soils.

A RATE-DEPENDENT TRIAXIAL BREAKAGE MODEL

The rate-independent triaxial breakage model by Einav (2007b) is here used as a reference for the extension to triaxial compression conditions. In its original formulation, the coupled breakage-plasticity dissipation rate function takes the following form:

$$\Phi(\dot{B},\dot{\varepsilon}_v^p,\dot{\varepsilon}_s^p)=\sqrt{\frac{E_B E_c}{(1-B)^2\cos^2\omega}\dot{B}^2+\frac{p^2}{(1-B)^2\sin^2\omega}\frac{E_c}{E_B}\dot{\varepsilon}_v^{p2}+M^2p^2\dot{\varepsilon}_s^{p2}} \tag{36}$$

where the volumetric and deviatoric plastic strains ε_v^p and ε_s^p are used as additional internal variables; ω is a factor controlling the coupling between plastic compaction and grain breakage; and *M* is the stress ratio at frictional failure. Since Equation (36) is first-order homogeneous in $\dot{B}$, $\dot{\varepsilon}_v^p$ and $\dot{\varepsilon}_s^p$, the predicted constitutive response is time independent. Under triaxial conditions, the total Helmholtz free energy has the form $\Psi=\Psi(B,\varepsilon_v^e,\varepsilon_s^e)$, with the volumetric and deviatoric elastic strains ε_v^e and ε_s^e playing the role of

external state variables. To consistently address multiple forms of energy dissipation, it is necessary to distinguish *generalized stresses* and *dissipative stress* (Houlsby and Puzrin, 2007). The generalized stresses are defined from the Helmholtz free energy:

$$p = \frac{\partial \Psi}{\partial \varepsilon_v^e}; q = \frac{\partial \Psi}{\partial \varepsilon_s^e}; E_B = -\frac{\partial \Psi}{\partial B} \tag{37}$$

while the dissipative stresses are defined from the dissipation potential z which is identical to Φ in this case:

$$\overline{p} = \frac{\partial \Phi}{\partial \dot{\varepsilon}_v^p}; \overline{q} = \frac{\partial \Phi}{\partial \dot{\varepsilon}_s^p}; \overline{E}_B = \frac{\partial \Phi}{\partial \dot{B}} \tag{38}$$

The yield criterion expressed in dissipative stresses can then be derived from the degenerated Legendre transform of (36) via (47) (Einav, 2007b):

$$\overline{y}_{pB}(\overline{E}_B, \overline{p}, \overline{q}) = \left(\frac{\overline{E}_B}{\frac{\sqrt{E_B E_c}}{(1-B)\cos\omega}} \right)^2 + \left(\frac{\overline{p}}{\frac{p}{(1-B)\sin\omega}\sqrt{\frac{E_c}{E_B}}} \right)^2 + \left(\frac{\overline{q}}{Mp} \right)^2 - 1 = 0 \tag{39}$$

A notable difference between the coupled breakage-friction dissipation rate function (36) and the one for pure breakage dissipation (19) is that the former involves three thermodynamic velocities $(\dot{B}, \dot{\varepsilon}_v^p, \dot{\varepsilon}_s^p)$ while the latter has only one (i.e., $\dot{B}$). The coupling of multiple dissipation mechanisms in (36) prevents the use of a generalization strategy based on the simple addition of a higher-order source of energy dissipation, ϕ_B. To circumvent such difficulty, the extension to multi-dissipative mechanisms is here tackled by directly postulating a flow potential w rather than one of the functions Φ or z. For this purpose, by analogy with Equation (27), a breakage-plastic overstress function for triaxial loading is defined as follows:

$$\overline{\xi}_{pB}(\overline{E}_B, \overline{p}, \overline{q}) = \left\langle \left(\frac{\overline{E}_B}{\frac{\sqrt{E_B E_c}}{(1-B)\cos\omega}} \right)^2 + \left(\frac{\overline{p}}{\frac{p}{(1-B)\sin\omega}\sqrt{\frac{E_c}{E_B}}} \right)^2 + \left(\frac{\overline{q}}{Mp} \right)^2 - 1 \right\rangle \tag{40}$$

The flow potential can then be defined in terms of $\overline{\xi}_{pB}(\overline{E}_B, \overline{p}, \overline{q})$, as follows:

$$w(\overline{E}_B, \overline{p}, \overline{q}) = \frac{E_c \dot{B}_0}{2\left(1-B\right)^2} \frac{\overline{\xi}_{pB}^{\,n/2+1}}{n/2+1} \tag{41}$$

which is similar to the form previously derived with reference to isotropic stress conditions (Equation (28)). The evolution equations can then be obtained through suitable derivatives of w with respect to $(\overline{E}_B, \overline{p}, \overline{q})$ and expressing them in the true stress space by exploiting the Ziegler's orthogonality condition in the form of $\overline{E}_B = E_B$, $\overline{p} = p$ and $\overline{q} = q$ (Nguyen and Einav, 2010b):

$$\dot{B} = \frac{\partial w}{\partial \overline{E}_B} = \dot{B}_0 \cos^2 \omega \xi_{pB}^{n/2} \tag{42a}$$

$$\dot{\varepsilon}_v^p = \frac{\partial w}{\partial \overline{p}} = \dot{B}_0 \frac{E_B}{p} \sin^2 \omega \xi_{pB}^{n/2} \tag{42b}$$

$$\dot{\varepsilon}_s^p = \frac{\partial w}{\partial \overline{q}} = \frac{\dot{B}_0 E_c}{\left(1-B\right)^2} \frac{q}{M^2 p^2} \xi_{pB}^{n/2} \tag{42c}$$

where

$$\xi_{pB}(E_B, p, q) = \left\langle \frac{\left(1-B\right)^2 E_B}{E_c} + \left(\frac{q}{Mp}\right)^2 - 1 \right\rangle \tag{43}$$

The relations above converge to the same breakage growth law in Equation (26) whenever isotropic stress conditions are imposed (q=0) and volumetric plastic dissipation is neglected (ω=0). Furthermore, by setting n = 2, Equations (42) lead to an overstress-based viscous model with a linear viscous nucleus function (Perzyna, 1966), which has already been used in previous studies of crushing-induced compaction localization for regularization purposes (Das et al., 2013). It is shown here that such regularization can be obtained from a thermomechanical procedure based on the flow potential. Moreover, from this analysis it

follows that the power law coefficient n should not be arbitrary selected, but it should rather coincide with the stress corrosion index of the constituting mineral (which is much larger than 2).

Finally, for a realistic representation of the elastic response of granular soils, one can adopt the following expression of Ψ that corresponds to a pressure-dependent elasticity model (Nguyen and Einav, 2010a):

$$\Psi(B,\varepsilon_v^e,\varepsilon_s^e)=(1-\vartheta B)\left[\frac{p_r}{\bar{K}(2-m)}\Lambda_v^{\frac{2-m}{1-m}}+\frac{3}{2}p_r\bar{G}\Lambda_v^{\frac{m}{1-m}}\varepsilon_s^{e2}\right] \tag{44}$$

where $\Lambda_v=\bar{K}(1-m)\varepsilon_v^e+1$; p_r is a reference pressure (here set to 1 kPa); $\bar{K}$ and $\bar{G}$ are non-dimensional elastic constants, and m describes the pressure dependence of the macroscopic elastic stiffness (here assumed to be 0.5).

MODEL VALIDATION

Rate effects in oedometric compression tests

The one-dimensional compression response of sand typically exhibits weak dependence on time and loading rate. An example of such dependences is illustrated by the oedometric tests conducted on Ottawa sand by De Souza (1958) , which suggest that the compression curves shift upwards when shorter time intervals (Δt) are allowed before applying the new stress increment (Figure 7a). Such processes can be simulated with the proposed triaxial model by applying constant lateral strain and increments of vertical stress. For this purpose, it has been assumed that each loading increment is applied within 1s, after which creep is allowed for different time intervals Δt that corresponds to those used in the experiments reported in Figure 7. The model parameters have been calibrated by using the following general procedure: (i) The grading index (ϑ=0.63) has been computed from data about the initial GSD. Similar to previous studies (e.g., Zhang and Buscarnera, 2014), a power law curve based on the reported value of initial mean grain size (D_{50}=0.28 mm) has been used to represent a uniform grading (see Appendix 2); (ii) Compression data has been used to infer the model constants that control the mechanical properties at the rate-independent limit. In this case, data

available for the longest loading interval (Δt=50 min) has been used to approximate the response at low strain rates. Specifically, the elastic properties ($\bar{K}$ and $\bar{G}$) have been obtained by matching the pre-yielding portion of the compression curve, while the parameters E_c, M and ω have been calibrated to match the yielding stress and the slope of the post-yielding branch; (iii) Evidences of rate-dependent response are eventually used to calibrate the constants of the newly proposed rate-dependent breakage model, n and $\dot{B}_0$. With reference to Figure 7, compression data for the shortest loading intervals (i.e., Δt= 2 min and 10 min) has been used to match the upward shift of the compression curves, as well as their shape.

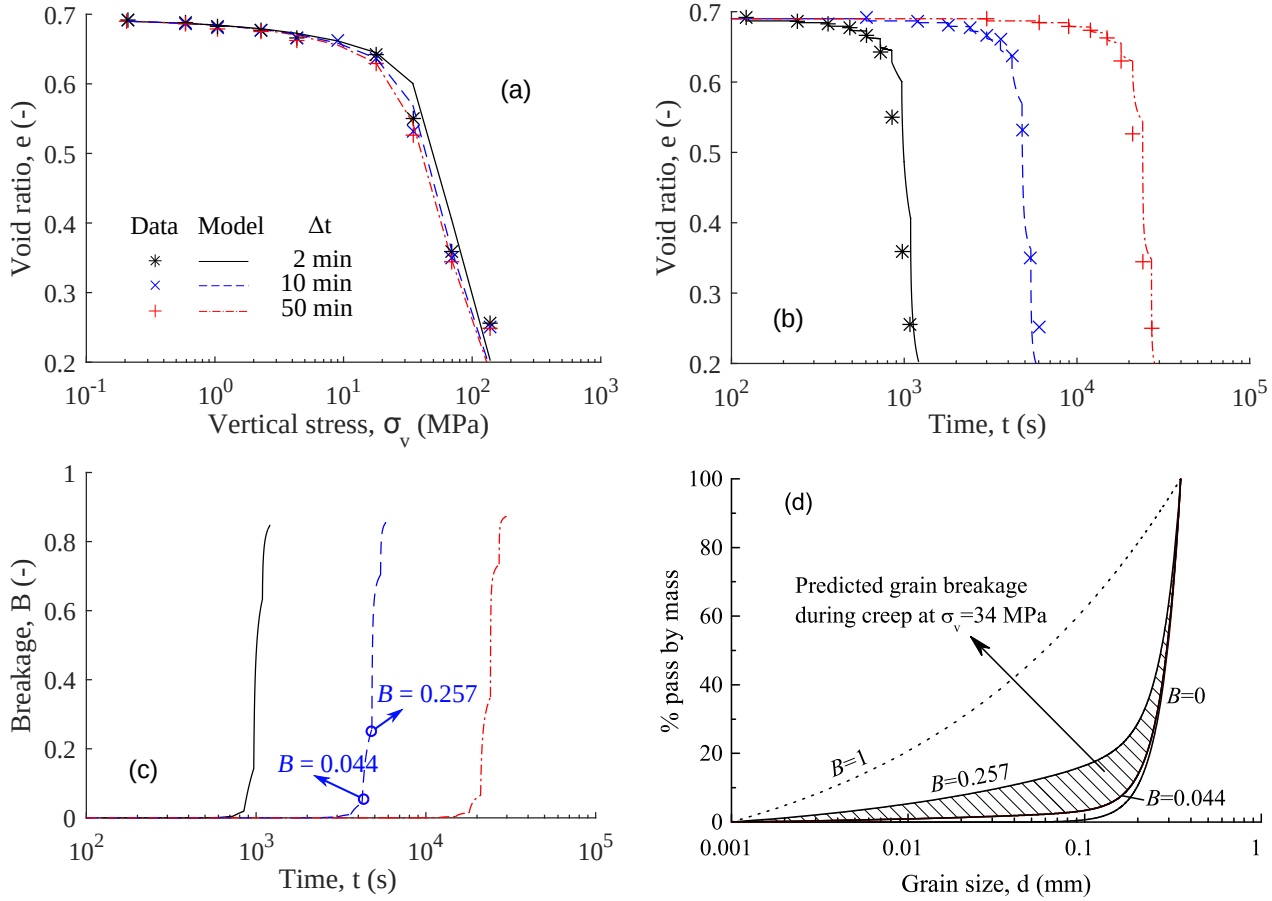

Figure 7: Data and model prediction of oedometric compression tests on Ottawa sand at different loading time intervals: a) Compression response (data from De Souza, 1958); b) void ratio evolution; c) breakage evolution; d) graphical representation of the evolution of B (shaded area) in presence of constant vertical stress (σ_v=34MPa; Δt=10min). Parameters used: ϑ=0.63, E_c=0.2 MPa and $\bar{K}$ =4500, $\bar{G}$ =4900, ω=67°, M=1.3, n=15 and $\dot{B}_0$ =2×10^{-4}/s.

Figure 7a compares model performance and experimental data on the e – log σ_v plane. The model is capable of capturing quantitatively both the compression responses and the weak rate-dependence emerging from

the high-pressure oedometer tests. The calibrated mechanical parameters (e.g. E_c, M and $\bar{K}$) are compatible with those typical found for a wide range of granular soils (Zhang and Buscarnera, 2014) and the viscous parameter n=15 falls in the range of stress corrosion index for quartz and quartz-rich rocks (Figure 1b). As is frequently observed from oedometer tests, the predicted void ratio history (Figure 7b) shows that creep deformations are non-negligible, especially at high stress levels. The computed void ratio at the end of each creep stage agrees well with the data reported on the e- log t plane, which confirmed the validity of the selected values of n and $\dot{B}_0$. For each compression test, the model also generates a breakage evolution curve (Figure 7c) which allows one to track the changes of the GSD. For example, for an Ottawa sand specimen under a sustained vertical stress of 34 MPa the breakage B is predicted to increase from 0.044 to 0.257 after Δt=10 min (Figure 7d). Although no data on the evolution of the GSD has been reported for this specific tests, similar patterns have been found in other experiments on crushable soils (e.g. Karimpour, 2012).

A more detailed evaluation of the rate-dependent characteristics predicted by the model can be gained by comparing the simulated creep strain histories with those measured at various loading increments. For this purpose, creep data from oedometric compression tests on a quartz sand reported by Takei et al. (2001) has been used (Figure 8). Again the grading index has been computed by using the reported grain size (D_{50}=1.43 mm) and assuming an initial uniform grading. Each load increment has been assumed to be applied in 1s, after which a creep stage was simulated. In addition, the parameters of the baseline breakage model ($\bar{K}$, $\bar{G}$ E_c, M and ω) have been calibrated through a strategy similar to that used for the previous example, while the parameters n and $\dot{B}_0$ have been selected to match the magnitude and rate of the measured creep response at a stress level of 20 MPa (Figure 8b). It can be noticed that the computed compression curves and the predicted strain histories at the other stress levels (σ_v =1.11 MPa ~ 9.95 MPa) exhibit an excellent agreement with the experiments. Such agreement has been achieved by using a power law coefficient n = 30, which is again within the range of values reported for typical rock-forming minerals. In addition, the negligible creep measured at the lowest stress levels (i.e. σ_v=1.11 MPa and 2.34 MPa) is correctly captured by the model,

thus reflecting that under high compressive stresses and constrained kinematic conditions grain crushing plays a dominant role in the accumulation of creep. Although other time-dependent processes may influence creep rates in granular soils (e.g., at low to intermediate stress levels, where grain damage may be negligible and/or coexist with other inelastic mechanisms), the model performance in this particular example validates the hypothesized link between delayed crack growth and macroscopic creep for cases in which grain crushing is the main source of microstructural rearrangement.

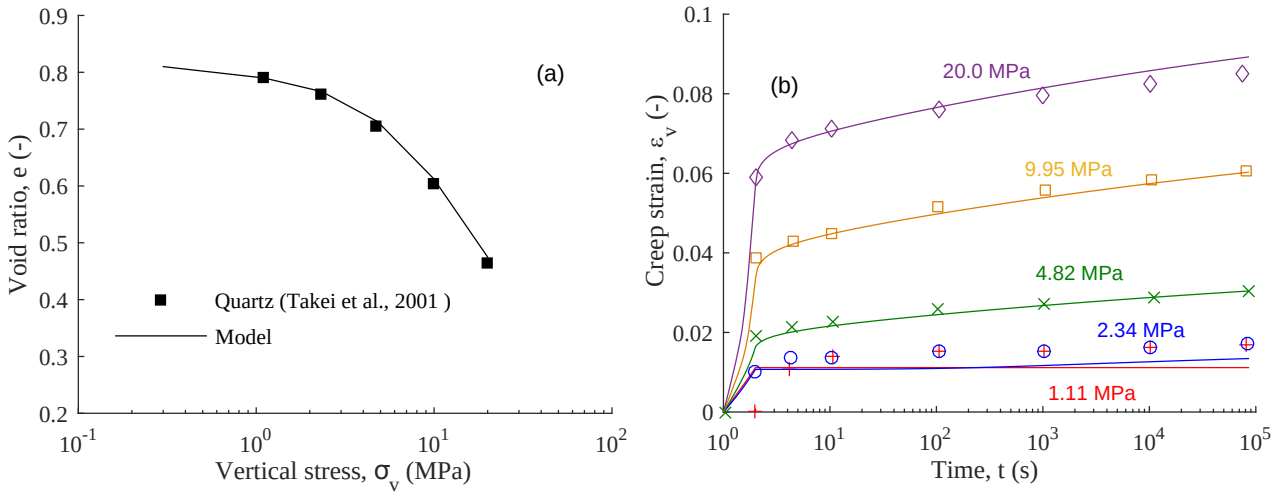

Figure 8: Data and model predictions of oedometric creep tests on quartz sand: a) compression response, b) creep response (data from Takei et al., 2001). Parameters used: ϑ=0.75, E_c=0.09 MPa and $\bar{K}$ =1500, $\bar{G}$ =1640, ω=15°, M=1.2, n=30 and $\dot{B}_0 = 2\times10^{-2}$/ s.

Rate effects in triaxial compression tests

Karimpour and Lade (2010, 2013, 2014) have recently performed a series of triaxial compression tests on saturated Virginia Beach sand under high confining pressures (8 MPa) to study the effect of the loading rate on its stress-strain, creep and relaxation responses. Such data are here used to validate the characteristics of the proposed model along stress paths that involve considerable shear strains. The strategy is to first calibrate all the model parameters based on stress-strain curves reported for various strain rates, then using the same set of parameters to predict stress relaxation responses to be compared with measured relaxation curves. Figure 9 presents measured and simulated stress-strain curves for constant strain rate triaxial tests, for which a calibration strategy similar to that discussed in the previous cases has been used to constrain

the model parameters. Stress relaxation tests are then simulated by interrupting each test at 2.8% strain level and then maintaining constant axial strain ε_a for one day, thus following exactly the procedure described by Lade and Karimpour (2014). The data in Figure 10a suggests that upon ceasing of axial straining, a drop of q manifests on the q-ε_a plane, while negligible volumetric changes occur during the relaxation stage. These characteristics have been successfully predicted by the model, though there is a slight over prediction of the volumetric compaction prior to the relaxation stage. Figure 10b presents the time history of q relaxation, as well as the absolute values of decreasing stress deviator. An excellent agreement between model predictions and experimental data is observed on both planes. More interestingly, the convergence of the three q-t curves after certain amount of relaxation time is successfully predicted by the proposed model.

Also for Virginia Beach sand a value of n =30 has been used, which again falls within the range of corrosion indices summarized in Figure 1b. These evidences suggest that high values of n are necessary to properly capture strain-rate sensitivity, creep and relaxation in granular soils at high pressures. Other values of n (e.g. classical Perzyna model with n=2) would instead not be able to match neither of these effects due to the high sensitivity of the response to small changes in strain rates (see section 4.3). Such observations indirectly validate the hypothesis in Equation (29), i.e. that the power law coefficient governing the breakage evolution is linked with the corrosion index controlling the growth of cracks in particles.

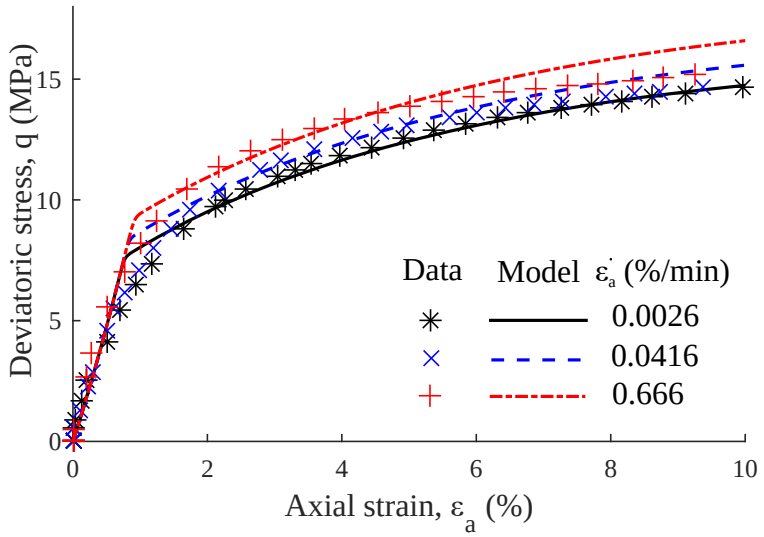

Figure 9: Experimental data and model simulations of the stress strain response of Virginia Beach sand subjected to various strain

rates at a confining pressure of 8 MPa (data from Karimpour and Lade, 2014). The grading index ϑ=0.72 results from the reported D_{50}=0.6 mm. The calibrated parameters are: E_c=0.12 MPa and $\bar{K}$ =4000, $\bar{G}$ =4360, ω=45°, M=1.02, n=30 and $\dot{B}_0$ =2×10^{-2}/s.

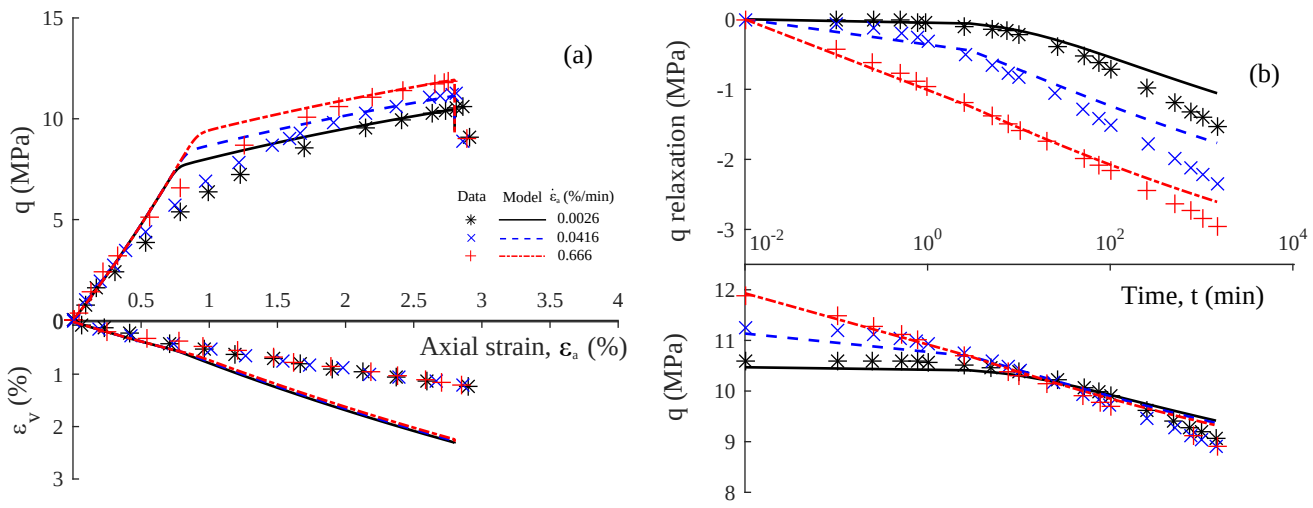

Figure 10: Experimental data and model simulations of triaxial relaxation tests on Virginia Beach sand (data from Karimpour and Lade, 2014): a) show the q and ε_v responses, b) presents the relative and absolute drop of q due to relaxation.

Nonisotach viscous behaviour of sand

The term *isotach* refers to viscous responses that can be well described through a unique stress-strain-strain rate relation. Clay typically follows a isotach behaviour (Tatsuoka et al., 2002), while the rate effect of sand cannot be characterized by such unique relation and it is thus referred to as *nonisotach*. Here to describe the characteristics of the model predictions we follow the procedure used by Lade and co-workers (Augustesen et al., 2004; Lade and Karimpour, 2014) to identify nonisotach behaviour in granular soils. First, a reference q-ε_a curve is defined with reference to a specific strain rate. Then, the test is repeated at the same strain rate but it is interrupted at different strain levels to perform creep and/or relaxation tests lasting 24 hours. The final points of these tests are reported on the q-ε_a plane and are used to define two curves (referred to as 1-day creep and 1-day relaxation curves). The coincidence of these curves indicates isotach viscous behaviour, while the lack of it reflects a nonisotach response. Figures 11 compares the results by Lade and Karimpour (2014) with model simulations of 1-day creep and 1-day relaxation curves for Virginia Beach sand based on the same parameters calibrated previously. It can be readily seen that the model captures the nonisotach behaviour exhibited by the sand (Figure 11b). Specifically, the predicted 1-day creep curve agrees well with

the measurements. By contrast, while the computed 1-day relaxation curve underpredicts the stress drops measured in the tests, it displays qualitative trends similar to those reported by the data. Figure 11c and d report measured and predicted time history of creep strain and stress relaxation. Again, excellent agreement is observed on creep strain histories at various levels of axial strain, while the predictions of stress relaxation can be considered to be satisfactory only from a qualitative standpoint. It is worth emphasizing that the good agreement between data and predictions in terms of rate-sensitive stress-strain response, creep, relaxation and nonisotach characteristics has been achieved in all cases by using a unique set of parameters with clear physical meanings. Such feature can be interpreted as a direct outcome of the proposed rate-dependent thermodynamic framework, which was constructed in light of the energetics of delayed fracture at the particle scale.

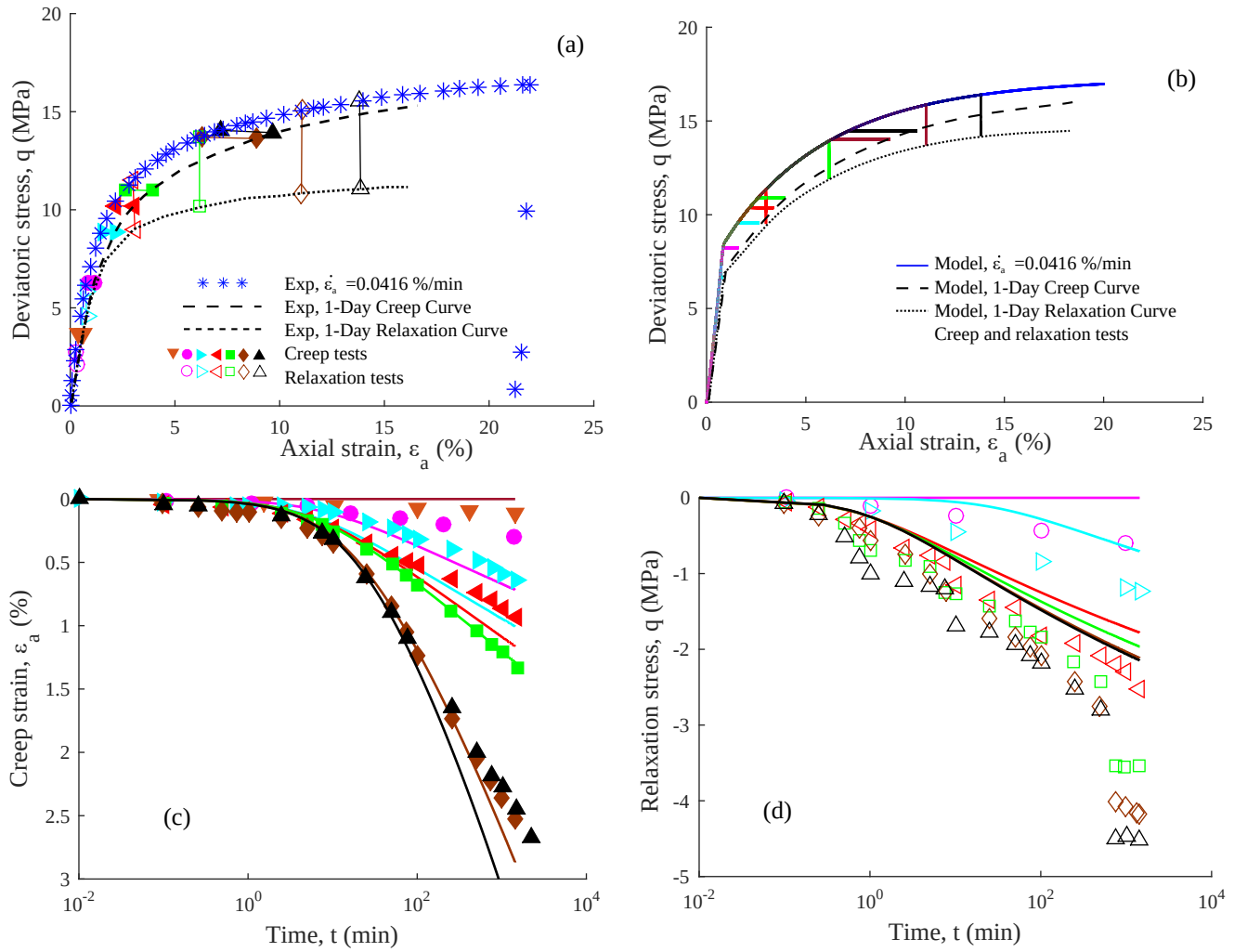

Figure 11: a) 1-day creep and relaxation curves reported by Lade and Karimpour (2014) and b) model computations simulating the same experimental procedure; c) measured and predicted history of creep strain and d) those of the relaxation stress.

CONCLUSIONS

A rate-dependent breakage model inspired by the thermodynamics of subcritical crack propagation has been proposed with the goal to simulate creep/relaxation processes dominated by delayed grain crushing. For this purpose, fracture kinetic theories have been recast in the framework of thermodynamics with internal variables. This has led to the identification of an additional term of energy dissipation which (i) augments the loss of energy by surface area creation and (ii) generates rate-sensitivity through a non-homogeneous dependence on the crack growth rate. The power law coefficient of such higher order function was found to be the corrosion index measured from subcritical fracture tests in brittle solids. Hence, by assuming that the rate effects of soil specimens under high pressures are controlled by the subcritical growth of cracks in individual particles, a new form of breakage dissipation has been proposed by incorporating the same degree of non-linearity found at the scale of intra-grain cracks. Such hypothesis has generated a continuum model in which the timing of delayed comminution is controlled by the same stress corrosion index used to describe the growth of individual particle flaws. A rate-dependent triaxial model has been finally formulated by coupling the breakage dissipation to both frictional and plastic dissipation, and it has been validated against a wide range of data for sands subjected to oedometric and triaxial compression conditions. The analyses have shown that the model exhibits excellent capacity of capturing complex patterns of soil response, including strain-rate sensitivity, creep histories, stress relaxation patterns and nonisotach viscous behaviour. All such features could be reproduced in all cases only by using a degree of nonlinearity of the viscous functions compatible with the values of corrosion index reported in the literature for quartz, silica and other rock-forming minerals. As a result, these findings validate the hypotheses about the major role played by subcritical crack growth processes on the macroscopic manifestation of rate-dependent crushing.

The present study differs from other elasto-viscoplastic modelling approaches for crushable granular soils in that it describes the rate-dependent behaviour of specimens by addressing the origin of changes of their physical characteristics over time at the scale of intra-grain cracks. Hence, it can provide support for the development of constitutive laws able to connect microscopic and macroscopic scales in granular materials, and offers at the same time a convenient platform to incorporate physico-chemical agents (e.g. relative humidity) affecting the crushability of granular systems exposed to changing environmental conditions.

REFERENCES

Atkinson, B. K. (1980) Stress corrosion and the rate-dependent tensile failure of a fine-grained quartz rock. *Tectonophysics* **65(3)**:281-290.

Atkinson, B. K. (1982) Subcritical crack propagation in rocks: theory, experimental results and applications. *Journal of Structural Geology* **4(1)**:41-56.

Atkinson, B. K. (1984) Subcritical crack growth in geological materials. *Journal of Geophysical Research: Solid Earth (1978–2012)* **89(B6)**:4077-4114.

Atkinson, B. K. & Meredith, P. G. (1987) The theory of subcritical crack growth with applications to minerals and rocks. *Fracture mechanics of rock* **2**:111-166.

Augustesen, A., Liingaard, M. & Lade, P. V. (2004) Evaluation of time-dependent behavior of soils. *International Journal of Geomechanics* **4(3)**:137-156.

Boudet, J., Ciliberto, S. & Steinberg, V. (1996) Dynamics of crack propagation in brittle materials. *Journal de Physique II* **6(10)**:1493-1516.

Buscarnera, G. (2012) A conceptual model for the chemo-mechanical degradation of granular geomaterials. *Géotechnique Letters* **2(3)**:149-154.

Buscarnera, G. & Das, A. (2015) Chemo‐mechanics of cemented granular solids subjected to precipitation and dissolution of mineral species. *International Journal for Numerical and Analytical Methods in Geomechanics*.

Buscarnera, G. & Einav, I. (2012) The yielding of brittle unsaturated granular soils. *Géotechnique* **62(2)**:147.

Chan, A. W.-K. (2004) Production-induced reservoir compaction, permeability loss and land surface subsidence.) Ph.D. thesis, Stanford University, Stanford, CA.

Charles, R. (1958) Static fatigue of glass. I. *Journal of Applied Physics* **29(11)**:1549-1553.

Collins, I. & Houlsby, G. (1997) Application of thermomechanical principles to the modelling of geotechnical materials. *Proceedings of the Royal Society of London A: Mathematical, Physical and Engineering Sciences* **453(1964)**:1975-2001.

Collins, I. & Muhunthan, B. (2003) On the relationship between stress–dilatancy, anisotropy, and plastic dissipation for granular materials. *Géotechnique* **53(7)**:611-618.

Das, A., Nguyen, G. D. & Einav, I. (2013) The propagation of compaction bands in porous rocks based on breakage mechanics. *Journal of Geophysical Research: Solid Earth* **118(5)**:2049-2066.

De Souza, J. (1958) Compressibility of sand at high pressure. *Massachusetts Institute of Technology, Massachusetts*.

Döll, W. (1984) Kinetics of crack tip craze zone before and during fracture. *Polymer Engineering & Science* **24(10)**:798-808.

Einav, I. (2007a) Breakage mechanics-part I: theory. *Journal of the Mechanics and Physics of Solids* **55(6)**:1274-1297.

Einav, I. (2007b) Breakage mechanics-Part II: Modelling granular materials. *Journal of the Mechanics and Physics of Solids* **55(6)**:1298-1320.
Einav, I., Houlsby, G. & Nguyen, G. (2007) Coupled damage and plasticity models derived from energy and dissipation potentials. *International Journal of Solids and Structures* **44(7)**:2487-2508.
Fisher, Q. J., Casey, M., Clennell, M. B. & Knipe, R. J. (1999) Mechanical compaction of deeply buried sandstones of the North Sea. *Marine and Petroleum Geology* **16(7)**:605-618.
Gao, S., Zhang, Y. D., Sonta, A. & Buscarnera, G. (2016) Evolution of the Water Retention Characteristics of Granular Materials Subjected to Grain Crushing. *Journal of Geotechnical and Geoenvironmental Engineering*:06016006.
Griffith, A. A. (1921) The phenomena of rupture and flow in solids. *Philosophical transactions of the royal society of london. Series A, containing papers of a mathematical or physical character* **221**:163-198.
Hackl, K. & Fischer, F. D. (2008) On the relation between the principle of maximum dissipation and inelastic evolution given by dissipation potentials. *Proceedings of the Royal Society of London A: Mathematical, Physical and Engineering Sciences* **464(2089)**:117-132.
Houlsby, G. & Puzrin, A. (2002) Rate-dependent plasticity models derived from potential functions. *Journal of Rheology (1978-present)* **46(1)**:113-126.
Houlsby, G. T. (2014) Dissipation rate functions, Pseudopotentials, Potentials and Yield Surfaces. In *Beyond the Second Law*.) Springer, pp. 73-95.
Houlsby, G. T. & Puzrin, A. M. (2007) *Principles of hyperplasticity: an approach to plasticity theory based on thermodynamic principles.* Springer Science & Business Media.
Karimpour, H. (2012) Time effects in relation to crushing in Sand.) The Catholic University of America, vol. Ph.D.
Karimpour, H. & Lade, P. V. (2010) Time effects relate to crushing in sand. *Journal of Geotechnical and Geoenvironmental Engineering* **136(9)**:1209-1219.
Lade, P. V. & Karimpour, H. (2014) Stress relaxation behavior in Virginia Beach sand. *Canadian Geotechnical Journal* **52(7)**:813-835.
Lade, P. V., Nam, J. & Liggio Jr, C. D. (2010) Effects of particle crushing in stress drop-relaxation experiments on crushed coral sand. *Journal of Geotechnical and Geoenvironmental Engineering* **136(3)**:500-509.
Leung, C., Lee, F. & Yet, N. (1997) The role of particle breakage in pile creep in sand. *Canadian Geotechnical Journal* **33(6)**:888-898.
Lubliner, J. (1972) On the thermodynamic foundations of non-linear solid mechanics. *International Journal of Non-Linear Mechanics* **7(3)**:237-254.
Maugis, D. (1985) Subcritical crack growth, surface energy, fracture toughness, stick-slip and embrittlement. *Journal of materials Science* **20(9)**:3041-3073.
Michalowski, R. L. & Nadukuru, S. S. (2012) Static fatigue, time effects, and delayed increase in penetration resistance after dynamic compaction of sands. *Journal of Geotechnical and Geoenvironmental Engineering* **138(5)**:564-574.
Michalske, T. A. & Freiman, S. W. (1982) A molecular interpretation of stress corrosion in silica. *Nature* **295**:511-512.
Nara, Y., Morimoto, K., Hiroyoshi, N., Yoneda, T., Kaneko, K. & Benson, P. M. (2012) Influence of relative humidity on fracture toughness of rock: implications for subcritical crack growth. *International Journal of Solids and Structures* **49(18)**:2471-2481.
Nguyen, G. D. & Einav, I. (2010a) The energetics of cataclasis based on breakage mechanics. In *Mechanics, Structure and Evolution of Fault Zones*.) Springer, pp. 1693-1724.
Nguyen, G. D. & Einav, I. (2010b) Nonlocal regularisation of a model based on breakage mechanics for granular materials. *International Journal of Solids and Structures* **47(10)**:1350-1360.
Oldecop, L. & Alonso, E. (2001) A model for rockfill compressibility. *Géotechnique* **51(2)**:127-139.

Oldecop, L. A. & Alonso, E. (2007) Theoretical investigation of the time-dependent behaviour of rockfill. *Géotechnique* **57(3)**:289-301.
Perzyna, P. (1966) Flmdamental Problems in Viseoplasticity. *Advances in applied mechanics* **9**:243.
Rice, J. (1978) Thermodynamics of the quasi-static growth of Griffith cracks. *Journal of the Mechanics and Physics of Solids* **26(2)**:61-78.
Rice, J. R. (1971) Inelastic constitutive relations for solids: an internal-variable theory and its application to metal plasticity. *Journal of the Mechanics and Physics of Solids* **19(6)**:433-455.
Scholz, C. H. (1972) Static fatigue of quartz. *Journal of Geophysical Research* **77(11)**:2104-2114.
Takei, M., Kusakabe, O. & Hayashi, T. (2001) Time-dependent behavior of crushable materials in one-dimensional compression tests. *Soils and foundations* **41(1)**:97-121.
Tatsuoka, F., Di Benedetto, H., Enomoto, T., Kawabe, S. & Kongkitkul, W. (2008) Various viscosity types of geomaterials in shear and their mathematical expression. *Soils and foundations* **48(1)**:41-60.
Tatsuoka, F., Ishihara, M., Di Benedetto, H. & Kuwano, R. (2002) Time-dependent shear deformation characteristics of geomaterials and their simulation. *Soils and foundations* **42(2)**:103-129.
Weidmann, G. & Holloway, D. (1974) Plastic flow-slow crack-propagation and static fatigue in glass. *Physics and Chemistry of Glasses* **15(3)**:68-75.
Wiederhorn, S. (1967) Influence of Water Vapor on Crack Propagation in Soda ‐ Lime Glass. *Journal of the American Ceramic Society* **50(8)**:407-414.
Wiederhorn, S. & Bolz, L. (1970) Stress corrosion and static fatigue of glass. *Journal of the American Ceramic Society* **53(10)**:543-548.
Yin, J.-H. & Graham, J. (1999) Elastic viscoplastic modelling of the time-dependent stress-strain behaviour of soils. *Canadian Geotechnical Journal* **36(4)**:736-745.
Zhang, Y. D. & Buscarnera, G. (2014) Grainsize dependence of clastic yielding in unsaturated granular soils. *Granular Matter* **16(4)**:469-483.
Zhang, Y. D., Buscarnera, G. & Einav, I. (2016) Grainsize dependence of yielding in granular soils interpreted using fracture mechanics, breakage mechanics and Weibull statistics. *Géotechnique* **66(2)**:149-160.
Ziegler, H. (1977) *An introduction to thermodynamics.* North-Holland Publishing Company.

APPENDIX 1: DISSIPATION FUNCTIONS AND POTENTIALS

In the framework of *thermodynamics with internal variables*, it is postulated that for a given system one can identify a set of external variables $\mathbf{A} = \{A_1, A_2, ...A_m\}$ (e.g., elastic strains), as well as a set of internal variables $\boldsymbol{\alpha} = \{\alpha_1, \alpha_1, ..., \alpha_n\}$ (e.g. damage, crack length) representing the state of the system. The energy dissipation rate caused by the thermodynamic velocities $\dot{\boldsymbol{\alpha}}$ can be expressed as:

$$\Phi(\mathbf{A}, \dot{\boldsymbol{\alpha}}) = \boldsymbol{\chi} : \dot{\boldsymbol{\alpha}} \geq 0 \tag{45}$$

where $\boldsymbol{\chi} = \{\chi_1, \chi_2, ...\chi_n\}$ are thermodynamic forces conjugated to $\dot{\boldsymbol{\alpha}}$. If it is assumed that $\dot{\boldsymbol{\alpha}}$ maximizes the dissipation rate, the direction of $\boldsymbol{\chi}$ can be defined from $\Phi(\mathbf{A}, \dot{\boldsymbol{\alpha}})$ by differentiation with respect to $\dot{\boldsymbol{\alpha}}$ (so-

called Ziegler's orthogonality condition, according to which $\boldsymbol{\chi}$ is orthogonal to a level set of Φ; Ziegler, 1977). Alternatively, the existence of a *force potential* $z(\mathbf{A},\dot{\boldsymbol{\alpha}})$ can be postulated (Houlsby, 2014), from which both magnitude and direction of $\boldsymbol{\chi}$ can be determined, as follows:

$$\boldsymbol{\chi} = \frac{\partial z}{\partial \dot{\boldsymbol{\alpha}}} \tag{46}$$

Furthermore, by performing a Legendre transformation of the force potential, it is possible to derive another potential function, $w(\mathbf{A},\boldsymbol{\chi})$, often referred to as *flow potential*:

$$w(\mathbf{A},\boldsymbol{\chi}) = \boldsymbol{\chi} : \dot{\boldsymbol{\alpha}} - z = \Phi - z \tag{47}$$

which by differentiation with respect to $\boldsymbol{\chi}$ provides the evolution equation law for $\boldsymbol{\alpha}$, as follows:

$$\dot{\boldsymbol{\alpha}} = \frac{\partial w}{\partial \boldsymbol{\chi}} \tag{48}$$

The dissipation rate function Φ and the potentials z and w are not independent of each other. In particular, for the case of Φ homogenous of degree one in $\dot{\boldsymbol{\alpha}}$ (i.e. $\Phi = (\partial\Phi / \partial\dot{\boldsymbol{\alpha}}) : \dot{\boldsymbol{\alpha}}$), the thermodynamic forces $\boldsymbol{\chi}$ can be expressed as:

$$\boldsymbol{\chi} = \frac{\partial \Phi}{\partial \dot{\boldsymbol{\alpha}}} \tag{49}$$

Comparing equations (46) and (49) it is readily apparent that Φ and z are identical. Another consequence of having both Φ and z homogenous of degree one in $\dot{\boldsymbol{\alpha}}$ is that w collapses to zero (i.e., w=0), thus defining a locus that bounds the reversible region of the space of the external state variables (the so called yield locus) and outside which the inelastic response of the system is modelled as a rate-independent process (Rice, 1971; Lubliner, 1972). While such particular case is the basis of many rate-independent thermomechanical models for geomaterials (Collins and Houlsby, 1997; Einav et al., 2007; Collins and Muhunthan, 2003), for the more general case of Φ homogeneous of degree $N > 1$ or non-homogenous function of $\dot{\boldsymbol{\alpha}}$, it can be

shown that the dissipation process becomes rate-dependent. For example, the case of N=2 corresponds to a linear viscoplastic behaviour (Perzyna, 1966), while N>2 or more complex non-homogenous functions lead to nonlinear viscoplastic theories (Houlsby and Puzrin, 2002). In these cases, the force potential z can be constructed from Φ by using the following relation (Hackl and Fischer, 2008; Houlsby and Puzrin, 2007):

$$z = \int_0^1 \frac{\Phi\left(\mathbf{A}, \tau\dot{\boldsymbol{\alpha}}\right)}{\tau} d\tau \tag{50}$$

where τ is a dummy variable. Conversely, if the force potential z is known, Φ can always be derived from the following relation:

$$\Phi\left(\mathbf{A}, \dot{\boldsymbol{\alpha}}\right) = \frac{\partial z\left(\mathbf{A}, \dot{\boldsymbol{\alpha}}\right)}{\partial \dot{\boldsymbol{\alpha}}} : \dot{\boldsymbol{\alpha}} \tag{51}$$

In both cases, the flow potential w can be obtained from (47). More generally, since Φ, z and w can be converted to each other via Equations (47), (50) and (51), it is sufficient to specify one of them to define the dissipative constitutive response (Houlsby, 2014).

APPENDIX 2: DEFINITION OF B AND COMPUTATION OF ϑ

This paper adopts the definition of relative breakage introduced by Einav (2007a). As a result, it assumes the existence of an ultimate fractal GSD (with fractal dimension $\alpha = 2.6$) which is achieved at large stresses during monotonic loading. The continuous transition from an initial to an ultimate GSD is modelled through the evolution of a breakage variable B, which is defined as the ratio between the area enclosed between current and initial GSDs (B_t) and the area enclosed between initial and ultimate GSDs (B_p). If fractional independence is further assumed (see Einav, 2007a), B can be expressed in terms of the GSD functions, as follows:

$$B=\frac{B_t}{B_p}=\frac{g_0(x)-g(x)}{g_0(x)-g_u(x)}=\frac{F_0(x)-F(x)}{F_0(x)-F_u(x)} \tag{52}$$

where g and F indicate the probability density functions and cumulative probability functions, respectively, while the subscripts 0 and u denote initial and ultimate GSDs.

The incorporation of the relations above into statistically homogenization procedures implies macroscopic constitutive functions which depend on the current location of the GSD. Such dependence is often reflected by grading index, such as ϑ, which takes into account the process of energy storage in the different grain fractions constituting an assembly (Einav, 2007a). Such grading index can be computed for arbitrary initial and ultimate GSDs by means of the following relation:

$$\vartheta=1-\frac{\int_{D_{\min}}^{D_{\max}} g_u(x)x^2dx}{\int_{D_{\min}}^{D_{\max}} g_0(x)x^2dx} \tag{53}$$

where D_{max} and D_{min} are the maximum and minimum grain sizes, respectively. For a particular expression of the GSD based on power law functions (Gao et al., 2016):

$$g_0(x)=\frac{(3-\beta)x^{2-\beta}}{D_{\max}^{3-\beta}-D_{\min}^{3-\beta}};\ g_u(x)=\frac{(3-\alpha)x^{2-\alpha}}{D_{\max}^{3-\alpha}-D_{\min}^{3-\alpha}} \tag{54}$$

the grading index can be readily computed by substituting (54) into (53):

$$\vartheta=1-\left(\frac{5-\beta}{3-\beta}\right)\left(\frac{3-\alpha}{5-\alpha}\right)\frac{\left(D_{\max}^{3-\beta}-D_{\min}^{3-\beta}\right)\left(D_{\max}^{5-\alpha}-D_{\min}^{5-\alpha}\right)}{\left(D_{\max}^{5-\beta}-D_{\min}^{5-\beta}\right)\left(D_{\max}^{3-\alpha}-D_{\min}^{3-\alpha}\right)} \tag{55}$$

In this work, the expression above has been used together with a power law coefficient β=1.5 (which reflects accurately a uniform initial grading prior to breakage).